Symmetric microwave potentials for interferometry with thermal atoms on a chip

Mahdi Ammar, Matthieu Dupont-Nivet, Landry Huet, Jean-Paul Pocholle, Peter Rosenbusch, Isabelle Bouchoule, Christoph I. Westbrook, Jérôme Estève, Jakob Reichel, Christine Guerlin, et al.

Symmetric microwave potentials for interferometry with thermal atoms on a chip

M. Ammar,[1,2] M. Dupont-Nivet,[1,3] L. Huet,[1] J.-P. Pocholle,[1] P. Rosenbusch,[4] I. Bouchoule,[3] C. I. Westbrook,[3] J. Estève,[2] J. Reichel,[2] C. Guerlin,[2] and S. Schwartz[1]

[1]*Thales Research and Technology France, Campus Polytechnique, 1 av. Fresnel, 91767 Palaiseau, France*

[2]*Laboratoire Kastler-Brossel, ENS, CNRS, Université Pierre et Marie Curie-Paris 6, 24 rue Lhomond, 75005 Paris, France*

[3]*Laboratoire Charles Fabry de l'Institut d'Optique, Campus Polytechnique, 2 av. Fresnel, 91127 Palaiseau, France*

[4]*LNE-SYRTE, Observatoire de Paris, UPMC, CNRS, 61 av de l'Observatoire, 75014 Paris, France*

(Received 9 December 2014; revised manuscript received 2 April 2015; published 26 May 2015)

A trapped atom interferometer involving state-selective adiabatic potentials with two microwave frequencies on a chip is proposed. We show that this configuration provides a way to achieve a high degree of symmetry between the two arms of the interferometer, which is necessary for coherent splitting and recombination of thermal (i.e., noncondensed) atoms. The resulting interferometer holds promise to achieve high contrast and long coherence time, while avoiding the mean-field interaction issues of interferometers based on trapped Bose-Einstein condensates.

DOI: 10.1103/PhysRevA.91.053623 PACS number(s): 03.75.Dg, 37.10.Gh, 37.25.+k

I. INTRODUCTION

Atom interferometers [1] have proven very successful in precision measurements such as the determination of the fine structure constant [2,3], the determination of the Newtonian gravitational constant [4], and inertial sensing of gravity [5], gravity gradients [6], and rotation [7]. They also show great promise to perform general relativity tests [8], including the weak equivalence principle [9,10].

In parallel, atom chips [11–14] provide a robust and versatile tool to trap and manipulate ultracold atoms, and are now routinely used in a variety of setups, including free-falling experiments in a drop tower [15] and compact atomic clocks [16]. In this context, they are very promising candidates for next-generation compact atomic sensors, including on-board applications [17]. However, while a variety of integrated beam splitters and coherent manipulation techniques have been demonstrated [18–25], none of the chip-based atom interferometers developed so far has reached metrological performance.

One of the initial problems encountered by atom-chip interferometers, namely the difficulty to maintain stable trapping and a reasonable trap-surface distance during the coherent splitting process [18,26], has been overcome by the use of dressed state adiabatic potentials [19,27]. However, another issue remains unresolved: trapped-atom interferometers using Bose-Einstein condensates (BECs) are especially sensitive to atom-atom interactions which induce phase diffusion, limiting their coherence time [28–30] and putting a serious constraint on the achievable precision in the measurement of the relative phase between the two arms of the interferometer [19,24].

One possible way to reduce the interaction strength, which we investigate throughout this paper, is the use of a trapped but thermal (i.e., nondegenerate) atomic cloud whose density is sufficiently low that the effect of interactions is negligible. This choice is somewhat analogous to using incoherent light in an optical interferometer, as already pointed out in [31] for guided thermal atoms propagating through two combined Y-shaped beam splitters. As in a "white light interferometer", the short coherence length of a thermal cloud (typically the thermal de Broglie wavelength [32]) requires that the interferometer be kept sufficiently symmetric (in a sense that will be defined in Sec. II) in order to observe any interference.

With this aim in view, we propose a protocol for a symmetric atom interferometer suitable for thermal atoms, using internal state labeling and adiabatic dressed potentials based on the same principle as in [22]. In the work of Ref. [22], which involves BECs, only one of the two internal states is dressed, breaking the spatial symmetry of the interferometer because the microwave field renders the trapping frequencies different for the two interferometer paths. To restore the symmetry, we propose the use of *two* microwave frequencies on *two* separate planar waveguides, each one interacting (primarily) with one of the two internal states. Thus each interferometer path can be individually controlled and made nearly identical to the other.

This paper is organized as follows: we first describe the proposed interferometric sequence, which brings us to discuss and quantify the role of symmetry in terms of interferometer contrast; we then describe the basic principles of the proposed protocol, and show why it is well suited for achieving a symmetric configuration; we then compare attractive and repulsive microwave fields, and show that the latter are much more favorable in this context; finally, taking into account how the atomic energy levels are affected by the presence of both static and microwave fields, we discuss the robustness of the design against external field fluctuations.

II. ROLE OF SYMMETRY IN THE INTERFEROMETER CONTRAST

To model a trapped atom interferometer, let us consider an ensemble of atoms with two internal states labeled $|a\rangle$ and $|b\rangle$. In the following we assume that $|a\rangle$ and $|b\rangle$ see two different time-dependent potentials V_a and V_b (a possible practical realization will be discussed in the next section). The evolution of such a system is ruled by the following Hamiltonian:

$$\widehat{H} = \widehat{p}^2/(2m) + V_a|a\rangle\langle a| + (V_b + \hbar\omega_{ab})|b\rangle\langle b|, \qquad (1)$$

where $\widehat{p}$ is the momentum operator and $\hbar\omega_{ab}$ is the energy difference between $|a\rangle$ and $|b\rangle$ at the beginning of the interferometric sequence t_i, where $V_a(t_i) = V_b(t_i)$. The atoms

are supposed to be initially prepared in $|a\rangle$, at thermal equilibrium with temperature T in the trapping potential V_a. The temperature T is moreover assumed to be high enough that Boltzmann statistics applies (for bosons in a harmonic trap with a BEC transition temperature T_c, this means that T is at least on the order of a few T_c, so that the gas is only weakly degenerate [33]). The atomic cloud can thus be described by the density matrix $\widehat{\rho}_{t_i} = \sum_n p_n |\psi_n(t_i)\rangle\langle\psi_n(t_i)|$, where $p_n = e^{-E_n^a(t_i)/(kT)}/Z$ are the Boltzmann factors, $Z = \sum_n e^{-E_n^a(t_i)/(kT)}$ is the partition function, $E_n^a(t)$ are the eigenenergies of $\widehat{H}|a\rangle\langle a|$, $|\psi_n(t)\rangle = |n_a(t)\rangle|a\rangle$ are the associated eigenvectors, and t_i is the initial time of the interferometric sequence [we also introduce the similar notations $E_n^b(t)$ and $|n_b(t)\rangle|b\rangle$ for the eigenenergies and eigenvectors of $\widehat{H}|b\rangle\langle b|$].

The atoms are then put into a coherent superposition of $|a\rangle$ and $|b\rangle$ with equal weight by applying a quasiresonant $\pi/2$ pulse, modeled by

$$|a\rangle \to \frac{|a\rangle - i e^{-i\phi}|b\rangle}{\sqrt{2}} \quad \text{and} \quad |b\rangle \to \frac{-i e^{i\phi}|a\rangle + |b\rangle}{\sqrt{2}}, \quad (2)$$

where $\phi = \phi_1$ is the phase of the electromagnetic field at the beginning of the $\pi/2$ pulse (for simplicity we have neglected the finite duration of the pulse). We also assume that $|a\rangle$ and $|b\rangle$ see identical trapping potentials before the beginning and after the end of the splitting process (for atoms trapped in dc magnetic fields, this means that $|a\rangle$ and $|b\rangle$ have identical magnetic moments), resulting in $|n_a(t_i)\rangle = |n_b(t_i)\rangle$ and $|n_a(t_f)\rangle = |n_b(t_f)\rangle$. The density matrix after this first $\pi/2$ pulse then reads $\widehat{\rho}_{t_i}^{(\pi/2)} = \sum_n p_n |\psi_n^{(\pi/2)}(t_i)\rangle\langle\psi_n^{(\pi/2)}(t_i)|$, with

$$\left|\psi_n^{(\pi/2)}(t_i)\right\rangle = \frac{|n_a(t_i)\rangle|a\rangle - i e^{-i\phi_1}|n_b(t_i)\rangle|b\rangle}{\sqrt{2}}. \quad (3)$$

The two internal states are then split and recombined by the time-dependent potentials $V_a(\widehat{z},t)$ and $V_b(\widehat{z},t)$ between t_i and t_f [with $V_a(t_i) = V_b(t_i)$ and $V_a(t_f) = V_b(t_f)$]. To describe the evolution of the system during this period, we assume that the time variations of the potentials $V_a(\widehat{z},t)$ and $V_b(\widehat{z},t)$ are slow enough that the adiabatic approximation can be applied (we will come back to this hypothesis in the case of time-dependent harmonic potentials later on in this section). We also neglect the effects of collisions and assume in particular that the atomic ensemble does not have time to re-thermalize between t_i and t_f. Under these approximations, the density matrix at t_f becomes $\widehat{\rho}_{t_f}^{(\pi/2)} = \sum_n p_n |\psi_n^{(\pi/2)}(t_f)\rangle\langle\psi_n^{(\pi/2)}(t_f)|$, with

$$\left|\psi_n^{(\pi/2)}(t_f)\right\rangle = \frac{e^{-i\phi_n^a}|n_a(t_f)\rangle|a\rangle - i e^{-i(\phi_n^b+\phi_1)}|n_b(t_f)\rangle|b\rangle}{\sqrt{2}},$$

where we have introduced the adiabatic phase factors $\phi_n^a = \int_{t_i}^{t_f} E_n^a(t)dt/\hbar + \gamma_n^a$ and $\phi_n^b = \int_{t_i}^{t_f} [E_n^b(t)/\hbar + \omega_{ab}]dt + \gamma_n^b$. In the latter expressions, $\gamma_n^{a,b}$ are the geometrical phase factors, or Berry phases [34]. In the following we make the additional hypothesis that the circuit in parameter space describing the changes in the potentials $V_a(\widehat{z},t)$ and $V_b(\widehat{z},t)$ retraces itself during the interferometer sequence, such that these geometrical phase factors vanish [34]. This is for example the case when the interferometric sequence has the additional temporal symmetry $V_{a,b}(\widehat{z},t_i + t) = V_{a,b}(\widehat{z},t_f - t)$ for all t between t_i and t_f, which we shall assume in the rest of this paper.

To close the interferometer, another $\pi/2$ pulse must be applied, modeled by (2) with $\phi = \phi_2$ the phase of the electromagnetic field at the beginning of this second $\pi/2$ pulse. This results in a final density matrix $\widehat{\rho}_f$, which can be used to compute the final population in $|a\rangle$ and $|b\rangle$, which are experimentally measurable by spectroscopy. For example, the population in $|a\rangle$ reads $p_a = \mathrm{Tr}(\widehat{\rho}_f|a\rangle\langle a|)$. All calculations done, this leads to

$$p_a = (1/2)\{1 - \mathrm{Re}[A(t_f)]\}, \quad (4)$$

with $A(t_f) = \sum_n p_n \exp[i(\phi_n^b - \phi_n^a + \phi_1 - \phi_2)]$. At this stage it is useful to introduce the frequency $\omega_{\pi/2}$ of the electromagnetic field driving the $\pi/2$ pulses, and the detuning $\Delta_{\pi/2} = \omega_{\pi/2} - \omega_{ab}$. This leads to the following expression for $A(t_f)$:

$$A(t_f) = e^{-i\Delta_{\pi/2}(t_f - t_i)} \sum_n p_n \exp\left\{\frac{i}{\hbar}\int_{t_i}^{t_f} \left[E_n^b(t) - E_n^a(t)\right]dt\right\}.$$

In Eq. (4) we identify the contrast as $C = |A|$ and the phase as $S = \arg(A)$ such that the measured signal reads $p_a = (1/2)[1 - C\cos(S)]$. In particular, the contrast can be written as

$$C = \left|\sum_n p_n \exp\left\{\frac{i}{\hbar}\int_{t_i}^{t_f} \left[E_n^b(t) - E_n^a(t)\right]dt\right\}\right|. \quad (5)$$

As can be seen in Eq. (5), the contrast is equal to unity if the eigenvalues of $\widehat{H}|a\rangle\langle a|$ and $\widehat{H}|b\rangle\langle b|$ are the same, which corresponds to the ideal case of a perfectly symmetric atom interferometer. In such a case, $S = \Delta_{\pi/2}(t_f - t_i)$ in the absence of any additional phase shift between the two arms of the interferometer, corresponding to the classical Ramsey signal.

To gain more physical insight from this model in the asymmetric case, it is instructive to consider the situation where the two potentials correspond to harmonic (one-dimensional) traps. We write the trapping potentials as

$$V_{a,b}(x,t) = \tfrac{1}{2}m\omega_{a,b}^2(t)[x - x_{a,b}(t)]^2, \quad (6)$$

where m is the atomic mass and $\omega_{a,b}$ and $x_{a,b}$ are, respectively, the frequency and the position of the harmonic trap created by $V_{a,b}$. In a typical interferometer sequence, $x_b - x_a$ will increase from zero to the maximum splitting distance x_0 between t_i and $t_i + \tau$ (splitting period), then the two traps will be held separate during a time T_h (holding period) and then $x_b - x_a$ will decrease from x_0 to zero in a time τ (recombination period), with $t_f - t_i = T_h + 2\tau$. Ideally, according to Eq. (5), this should be done while maintaining $\omega_a = \omega_b$ throughout the whole interferometric sequence to ensure a contrast equal to unity. However, to model residual asymmetries, we shall assume that $\omega_b - \omega_a$ grows linearly from ω to $\omega + \delta\omega$ [with $|\delta\omega| \ll \omega \equiv (\omega_a + \omega_b)/2$] during the splitting period, then stays equal to $\delta\omega$ during the holding time T_h and eventually decreases from $\delta\omega$ to zero during recombination. Under these hypotheses, an analytic expression for the contrast can be derived from Eq. (5), which reads

$$C = \frac{1 - \lambda}{\sqrt{(1-\lambda)^2 + 4\lambda\sin^2[\delta\omega(T_h + \tau)/2]}}, \quad (7)$$

with $\lambda = \exp[-\hbar\omega/(kT)]$. From the latter expression, it can be shown that the contrast depends on the duration of the interferometric sequence via the parameter $T_h + \tau$. In particular, it is reduced to $1/2$ when $T_h + \tau = \sqrt{3}\hbar\omega/(kT|\delta\omega|)$, which puts a limit on the coherence time of the thermal atom interferometer. Neglecting numerical factors on the order of unity, the limit on the coherence time induced by asymmetry thus takes the following simple and intuitive form:

$$t_c \simeq \frac{\hbar\omega}{|\delta\omega|kT}. \tag{8}$$

Equation (8) is the main result of this section. It shows that t_c increases with the degree of symmetry (measured by $|\delta\omega|/\omega$) and decreases when temperature increases, as expected intuitively. As an example, we obtain $t_c \simeq 15$ ms for a temperature of 500 nK and a degree of symmetry on the order of $\omega/\delta\omega \simeq 10^3$. Furthermore, Eq. (5) can be used to quantitatively analyze other defects, for example anharmonic potentials.

It can be noticed in Eq. (7) that the contrast revives for integer values of $\delta\omega(T_h + \tau)/(2\pi)$. However, we expect these revivals not to appear in practice when other trapping directions and experimental sources of noise are taken into account.

Interestingly, assuming harmonic potentials throughout the interferometer sequence also provides a more intuitive expression for the adiabatic hypothesis on V_a and V_b made to derive the results of this section. More precisely, starting from (6), the adiabaticity condition for a given eigenstate $|n(t)\rangle$ of $\widehat{H}|a\rangle\langle a|$ or $\widehat{H}|b\rangle\langle b|$ reads

$$\left|\langle n|\frac{\partial}{\partial t}|m\rangle\right| \ll |m-n|\omega \quad \forall m \neq n, \tag{9}$$

where we have used the fact that $\omega_a \simeq \omega_b \simeq \omega$. For the potentials written in (6), the latter expression translates into the following more intuitive conditions:

$$n\dot{\omega} \ll \omega^2 \quad \text{and} \quad n\frac{\dot{x}_{a,b}}{\sqrt{\langle x^2\rangle}} \ll \omega, \tag{10}$$

where $\sqrt{\langle x^2\rangle}$ is the average size of the thermal cloud given by $\sqrt{kT/(m\omega^2)}$. It seems reasonable to impose that the latter conditions must be fulfilled for all values of n up to the highest significantly populated level N, given by $N \simeq kT/(\hbar\omega)$. This provides a global adiabaticity condition for the interferometer in the harmonic case.

The simple model presented in this section illustrates the importance of symmetry to maintain the coherence of the interferometer. As already discussed in the Introduction, this can be seen as an atomic equivalent of white light interferometry in optics, where the path length between the two arms of the interferometer has to be made smaller than the coherence length. This is the main motivation for introducing the protocol of Sec. III, which aims to achieve symmetrical state-dependent potentials using microwave dressing with two different frequencies on an atom chip.

III. PROPOSAL OF A SYMMETRIC CONFIGURATION

A. Basic principle of the protocol

We consider in the following the experimental situation in which the $|F = 1, m_F = -1\rangle$ and $|F = 2, m_F = 1\rangle$ hyperfine

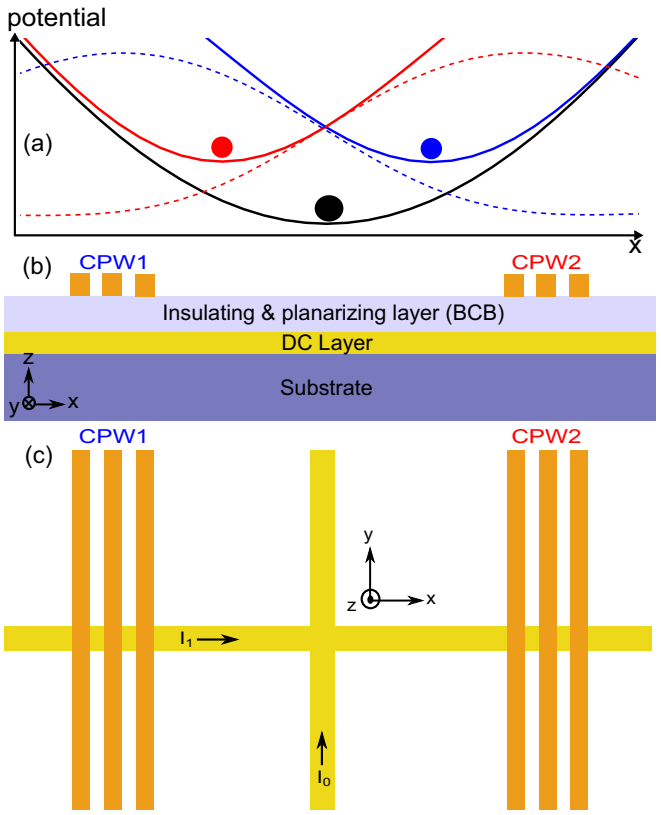

FIG. 1. (Color online) Basic principle of state-selective symmetrical splitting with two coplanar waveguides and two frequencies. (a) Typical shapes of the adiabatic potentials in the near field of the coplanar waveguides (CPWs), which is a symmetric version of the protocol demonstrated in [22] (see Fig. 3.c therein). The black line is the common initial trapping potential $[V_a(t_i)]$. The dashed curves represent (at least in the limit of large detunings) the potential barriers created by the microwave fields near the coplanar waveguides. The solid red and blue curves represent the resulting potentials for $|a\rangle$ and $|b\rangle$ (V_a and V_b). (b) Cut of the atom chip showing the CPWs and the dc layer, separated by an insulating and planarizing material. (c) Top view of the atom chip. The central wires that carry the static currents I_0 and I_1 are used to create a static microtrap in the vicinity of the atom chip. The CPWs are deposited on both sides of the trap center, at equal distance from the central wire carrying I_0.

levels of the $5^2S_{1/2}$ ground state of ^{87}Rb are used to implement the interferometric sequence described in the previous section (with $|F = 1, m_F = -1\rangle \equiv |a\rangle$ and $|F = 2, m_F = 1\rangle \equiv |b\rangle$). These two states have nearly identical magnetic moments, rendering their superposition robust against magnetic field fluctuations [35] and making the achievement of symmetric potentials easier, as will be described later on in this section. The $\pi/2$ pulses described in the previous section are produced by two-photon (microwave and radio-frequency) pulses, as demonstrated in [35]. Initially, the potential $V_a(t_i) = V_b(t_i)$ results from conventional dc magnetic trapping by the atom chip and external coils. Then, the interferometric sequence (splitting, holding, and recombination) is created by microwave dressing from two coplanar waveguides on the atom chip, as illustrated in Fig. 1(a). As already discussed in the Introduction, this protocol is a generalization of [22] with two

microwave frequencies on two separate coplanar waveguides (each one interacting mostly with one of the two states), with the goal of making the trapping potentials as symmetric as possible, as will be described in Sec. III C. The typical time sequence is as follows: the microwave fields are ramped from zero up to their maximum power during the splitting phase, are kept constant during the holding phase, and are gradually ramped down to zero during the recombination phase. The changes in the microwave power has to be slow enough to fulfill the adiabatic conditions both on the external states (as discussed in the previous section) and on the internal states (as will be discussed in the following section).

B. Adiabatic dressed-state potentials

In the presence of a dc magnetic field combined with a microwave field close to the hyperfine splitting frequency, the three Zeeman sublevels of $|F=1\rangle$ are coupled to the five Zeeman sublevels of $|F=2\rangle$, leading to dressed eigenstates [36].

Let us first consider the dressing on one two-level transition, where a state $|F=1,m_1\rangle \equiv |g\rangle$ is significantly coupled to only one state $|F=2,m_2\rangle \equiv |e\rangle$ by a microwave field with frequency ω. The coupling strength is given by the Rabi frequency Ω, which is proportional to the amplitude of the microwave magnetic field, and assumed to be much smaller than the Larmor frequency ω_L [i.e., the splitting with neighboring Zeeman sublevels, given by $\omega_L = \mu_B B/(2\hbar)$, B being the modulus of the dc magnetic field and μ_B the Bohr magneton] to ensure the validity of the two-level approximation. The energies of the resulting dressed states $|\pm\rangle$ are [37]

$$E_\pm = \frac{E_g+E_e}{2} \pm \frac{\hbar}{2}\sqrt{\Omega^2+\Delta^2} + \text{const}, \tag{11}$$

where E_g (respectively E_e) is the energy of the uncoupled level $|g\rangle$ (respectively $|e\rangle$), $\Delta = \omega - (E_e - E_g)/\hbar$ is the detuning, and the constant term accounts for the energy of the microwave field [38].

In the absence of any coupling ($\Omega = 0$) the state $|g\rangle$ corresponds to the dressed state $|+\rangle$ or $|-\rangle$ depending on the detuning. As long as the coupling is varied adiabatically the atoms will remain in a single dressed state. The adiabatic condition reads [39]

$$|\dot{\Omega}\Delta| \ll (\Delta^2+\Omega^2)^{3/2}. \tag{12}$$

Very importantly, condition (12) shall not be confused with the adiabatic condition used in the previous section to describe the dynamics of the interferometer: the latter was related to the changes in the trapping potentials V_a and V_b, while condition (12) is on the internal dynamics of the atoms. It results in the following adiabatic potential:

$$V_g = \frac{E_g+E_e}{2} + S_\Delta \frac{\hbar}{2}\sqrt{\Omega^2+\Delta^2} - \frac{\hbar\omega}{2}, \tag{13}$$

where S_Δ is the initial sign of Δ (which we assume to be constant over the spatial extent of the atomic cloud). Similarly, the adiabatic potential for atoms initially in the bare state $|e\rangle$ reads

$$V_e = \frac{E_g+E_e}{2} - S_\Delta \frac{\hbar}{2}\sqrt{\Omega^2+\Delta^2} + \frac{\hbar\omega}{2}. \tag{14}$$

In Eqs. (13) and (14), the average energy of the microwave field (in the sense of the semiclassical limit) has been removed, keeping only a $-\hbar\omega/2$ (respectively $+\hbar\omega/2$) term such that V_g (respectively V_e) coincides with E_g (respectively E_e) when Ω is initially set to zero.

C. Symmetric microwave dressing

We now consider the situation in which two microwave frequencies are used to shift the energies of two pairs of levels, in order to achieve a microwave-induced, state-dependent potential. These two frequencies are injected into two different coplanar waveguides (labeled CPW_1 and CPW_2) placed on either side of the dc magnetic trap center, as sketched in Figs. 1(b) and 1(c). One possible implementation to make the potentials symmetric, illustrated in Fig. 2, is to tune ω_1 such that it is mostly resonant with the transition between $|a\rangle$ and $|F=2,m_F=-1\rangle \equiv |c\rangle$, while ω_2 is tuned to be mostly resonant with the transition between $|b\rangle$ and $|F=1,m_F=1\rangle \equiv |d\rangle$. These conditions can be rewritten as $|\omega_1 - (E_c - E_a)/\hbar| \ll \omega_L$ and $|\omega_2 - (E_b - E_d)/\hbar| \ll \omega_L$, where E_c (respectively E_d) is the energy of the bare state $|c\rangle$ (respectively $|d\rangle$), and ω_L is the Larmor frequency, defined in the previous section. If we furthermore assume that the amplitude of the microwave magnetic field is much smaller than B (which means that all the Rabi frequencies corresponding to couplings between Zeeman sublevels of $F=1$ and $F=2$ are much smaller than ω_L), then the two-level approximation can be used for the

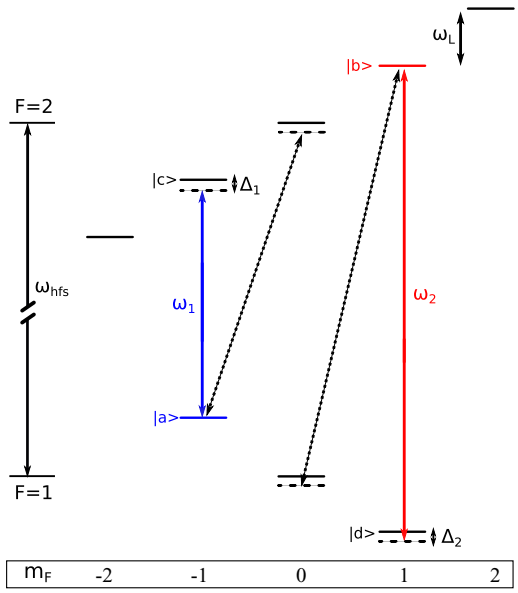

FIG. 2. (Color online) Energy levels of the $5^2S_{1/2}$ ground state of ^{87}Rb in the presence of a static magnetic field. To generate symmetrical state-dependent potentials, two microwave fields are used to couple the clock states $|a\rangle$ and $|b\rangle$ to two auxiliary states. Two combinations are possible by an appropriate choice of the microwave frequencies using either π (solid line) or σ transitions (dashed line). The π (respectively σ) transitions correspond to the case where the microwave and dc magnetic fields are parallel (respectively orthogonal). Both configurations can be readily achieved for example using a regular dimple trap [38].

transitions $|a\rangle \leftrightarrow |c\rangle$ and $|b\rangle \leftrightarrow |d\rangle$. Following Sec. III B, the adiabatic potential for the internal state initially in $|a\rangle$ then reads

$$V_a = \frac{E_a + E_c}{2} - \frac{\hbar\omega_1}{2} + S_{\Delta_1}\frac{\hbar}{2}\sqrt{\Omega_1^2 + \Delta_1^2}, \qquad (15)$$

where $\Delta_1 = \omega_1 - (E_c - E_a)/\hbar$ and Ω_1 is the Rabi frequency associated with the transition $|a\rangle \leftrightarrow |c\rangle$ and the microwave field at frequency ω_1. Similarly, the adiabatic potential for the internal state initially in $|b\rangle$ is

$$V_b = \frac{E_b + E_d}{2} + \frac{\hbar\omega_2}{2} - S_{\Delta_2}\frac{\hbar}{2}\sqrt{\Omega_2^2 + \Delta_2^2}, \qquad (16)$$

where $\Delta_2 = \omega_2 - (E_b - E_d)/\hbar$ and Ω_2 is the Rabi frequency associated with the transition $|b\rangle \leftrightarrow |d\rangle$ and the microwave field at frequency ω_2. The matrix elements of the interaction Hamiltonian associated with the transitions $|a\rangle \leftrightarrow |c\rangle$ and $|b\rangle \leftrightarrow |d\rangle$ are almost equal [38], which means that equivalent magnetic fields will lead to identical Rabi frequencies.

The energy of the bare states $|a\rangle, |b\rangle, |c\rangle$, and $|d\rangle$ can be approximated to the first order in B (neglecting the coupling between the nuclear angular momentum and the magnetic field) by the usual linear Zeeman formula, namely $E_a = \hbar\omega_L$, $E_b = \hbar\omega_{\rm hfs} + \hbar\omega_L$, $E_c = \hbar\omega_{\rm hfs} - \hbar\omega_L$, and $E_d = -\hbar\omega_L$, where $\omega_{\rm hfs} \simeq 2\pi \times 6.83$ GHz [40] is the zero-field hyperfine splitting (the common energy offset has been discarded). We furthermore impose that ω_1 and ω_2 be symmetrically tuned with respect to $\omega_{\rm hfs}$, a condition which can be written as $\omega_1 = \omega_{\rm hfs} - \Delta_0$ and $\omega_2 = \omega_{\rm hfs} + \Delta_0$. This implies in particular that the initial detunings Δ_1 and Δ_2 have equal absolute values and opposite signs (we denote by S the initial sign of $\Delta_1 = 2\omega_L - \Delta_0$). Equations (15) and (16) then read

$$V_a(\mathbf{r}) = \frac{\hbar\Delta_0}{2} + S\frac{\hbar}{2}\sqrt{\Omega_1^2(\mathbf{r}) + [2\omega_L(\mathbf{r}) - \Delta_0]^2} \qquad (17)$$

and $V_b(\mathbf{r}) = \hbar\omega_{\rm hfs} + \tilde{V}_b(\mathbf{r})$, with

$$\tilde{V}_b(\mathbf{r}) = \frac{\hbar\Delta_0}{2} + S\frac{\hbar}{2}\sqrt{\Omega_2^2(\mathbf{r}) + [2\omega_L(\mathbf{r}) - \Delta_0]^2}. \qquad (18)$$

Let us now consider the spatial dependence of V_a and V_b along the x axis of Fig. 1 in the framework of a simplified one-dimensional model. The dc magnetic trap is assumed to be harmonic and centered around $x = 0$, such that $\omega_L(x) = \omega_L(-x)$. The two coplanar waveguides are assumed to be at the same distance on either side of the origin and fed with the same microwave power, such that $\Omega_1(x) = \Omega_2(-x)$ (recall that the interaction Hamiltonian has almost the same matrix elements for the two transitions). This leads to $V_a(x) = \tilde{V}_b(-x)$ which satisfies the desired symmetry condition. This is the main result of this section, showing that symmetry, in the sense defined in Sec. II, is in principle possible with this configuration. This result can be generalized to the case of a more realistic geometry for the dc trap in three dimensions. In this case, the potentials V_a and V_b are found to be symmetric in the sense that they form two traps with similar eigenenergies.

One possible limitation of symmetry in this configuration is the presence of other (far off-resonance) transitions, although their effect is expected to be reduced at least by a factor on the order of $|\Delta_1|/\omega_L \ll 1$ as compared to the main $|a\rangle \leftrightarrow |c\rangle$ and $|b\rangle \leftrightarrow |d\rangle$ transitions, and can in principle be compensated by adjusting the power and frequency of the microwave dressing fields.

An alternative to the protocol described in this section is to use the σ_+ transitions $|a\rangle \leftrightarrow |F = 2, m_F = 0\rangle$ and $|b\rangle \leftrightarrow |F = 1, m_F = 0\rangle$ rather than $|a\rangle \leftrightarrow |c\rangle$ and $|b\rangle \leftrightarrow |d\rangle$, as illustrated by the dashed arrows of Fig. 2. We will not consider this alternative in detail in the following, but most of the results described in this paper can be transposed to it.

IV. ATTRACTIVE VERSUS REPULSIVE MICROWAVE FIELDS

It can be seen in Eqs. (17) and (18) that when the initial sign S of the detuning Δ_1 is positive, both levels $|a\rangle$ and $|b\rangle$ will be blueshifted: a maximum in the Rabi frequency $\Omega_{1,2}$ will result, for a constant value of the detuning $\Delta_1 = 2\omega_L - \Delta_0$, in a maximum of the adiabatic potential $V_{a,b}$ [as pictured in Fig. 1(a)]. Consequently, the microwave field will be called "repulsive" in this case. In the opposite case ($S < 0$), the microwave field will be called "attractive."

An important difference between repulsive and attractive microwave fields is the fact that the trap depth is limited in the latter case. This can be understood by first noticing that the Larmor frequency ω_L is minimal at the dc trap center, and increases with the distance from the center. In the attractive case, the detuning $\Delta_1 = 2\omega_L - \Delta_0$ is initially negative at the trap center, so it will go to zero for the points $\mathbf{r}$ in space corresponding to $\omega_L(\mathbf{r}) = \Delta_0/2$, giving rise to an avoided crossing. Beyond this point, the magnetic dependence of the adiabatic potentials $\partial V_{a,b}/\partial B$ changes sign, and the atoms beyond this limit are no longer trapped by the dc field. This puts a limitation on the typical temperature that can be used in the attractive case, typically $kT \ll \hbar\Delta_0$. Conversely, in the repulsive case, the detuning Δ_1 does not go to zero because it is initially positive at the trap center. The latter temperature constraint is thus relaxed.

A second reason to favor repulsive potentials arises from the fact that the atoms are trapped in a region of weaker microwave field than in the attractive case, reducing the mixing of the atomic levels, as discussed in the next section.

V. ROBUSTNESS TO MAGNETIC FIELD FLUCTUATIONS

In Sec. III C we have approximated the hyperfine energy levels of ^{87}Rb by the linear Zeeman formula, keeping only first order terms in $B \ll \hbar\omega_{\rm hfs}/\mu_B$ and neglecting the coupling between the nuclear angular momentum and the magnetic field based on the fact that the electron spin g factor is typically 3 orders of magnitude bigger than the nuclear spin g factor. However, the latter is not negligible when superpositions of internal states are considered, because even a small difference in the magnetic dependence of the energy levels can strongly affect coherence in the presence of magnetic field noise. A remarkable situation occurs for the $|F = 1, m_F = -1\rangle$ and $|F = 2, m_F = 1\rangle$ hyperfine levels of the $5^2S_{1/2}$ ground state of ^{87}Rb (labeled $|a\rangle$ and $|b\rangle$ in this paper), whose energy difference is independent of B to first order for a particular value $B_m \simeq 3.23$ G called the "sweet spot" [35,41], making their coherent superpositions particularly robust to magnetic field fluctuations. In this section we study the existence

conditions for this sweet spot and, when applicable, the changes in the value of B_m in the presence of microwave dressing.

To do this, we use the Breit-Rabi formula [40] for the hyperfine energy levels. Considering the fact that for most atomic physics experiments the magnetic field B is typically much smaller than $\hbar\omega_{\rm hfs}/\mu_B \simeq 0.5$ T, the energy levels for $F = 1$ can be approximated up to the second order in $\mu_B B/(\hbar\omega_{\rm hfs})$ by

$$E_{1,m_F} = \frac{m_F \mu_B B}{4}(5g_I - g_J) - \frac{\mu_B^2 \alpha (g_J - g_I)^2 B^2}{4\hbar\omega_{\rm hfs}}, \quad (19)$$

where $\alpha = 1 - m_F^2/4$. Similarly, the energy levels for $F = 2$ read $E_{2,m_F} = \tilde{E}_{2,m_F} + \hbar\omega_{\rm hfs}$, with

$$\tilde{E}_{2,m_F} = \frac{m_F \mu_B B}{4}(3g_I + g_J) + \frac{\mu_B^2 \alpha (g_J - g_I)^2 B^2}{4\hbar\omega_{\rm hfs}}. \quad (20)$$

In these formulas $g_J \simeq 2.002$ and $g_I \simeq -9.95 \times 10^{-4}$ are, respectively, the electron and the nuclear spin g factors [40]. In the absence of microwave dressing, the usual sweet spot for $|a\rangle$ and $|b\rangle$ can be readily retrieved from Eqs. (19) and (20) as the value of the magnetic field B_m^0 minimizing the energy difference $E_{2,1} - E_{1,-1}$, namely

$$B_m^0 = \frac{-8 g_I \hbar\omega_{\rm hfs}}{3\mu_B (g_J - g_I)^2} \simeq 3.23 \text{ G}. \quad (21)$$

Let us now assume that we start from a situation with $B = B_m^0$ in the absence of microwave power, and that we then gradually ramp the Rabi frequencies $\Omega_1 = \Omega_2$ up to a maximum value Ω. The relevant energy levels (corresponding to the π transitions of Fig. 2) are then $E_a = E_{1,-1}$, $E_b = E_{2,1}$, $E_c = E_{2,-1}$, and $E_d = E_{1,1}$ (which include, as we have mentioned, the full Breit-Rabi formula [40]). It is convenient to specify the values of ω_1 and ω_2 via the initial detunings $\Delta_1^0 = \omega_1 - (E_c^0 - E_a^0)/\hbar$ and $\Delta_2^0 = \omega_2 - (E_b^0 - E_d^0)/\hbar$, where the notation X^0 refers to the value of X at $B = B_m^0$. The problem can then be described by the two dimensionless parameters δ and κ, defined by

$$\delta = \Delta_1^0/\omega_L^0 = -\Delta_2^0/\omega_L^0 \quad \text{and} \quad \kappa = \left|\frac{\Omega}{\Delta_1^0}\right|, \quad (22)$$

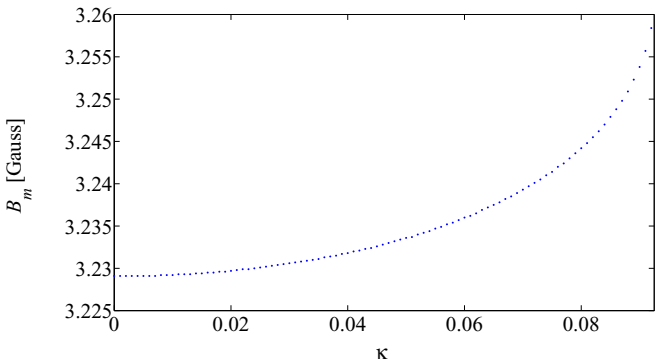

FIG. 3. (Color online) Numerically computed value of the sweet spot B_m [defined as the minimum of $V_b(B) - V_a(B)$] as a function of κ, with $\delta = -0.1$. The sweet spot remains up to a critical value on the order of $\kappa_c \simeq 0.092$.

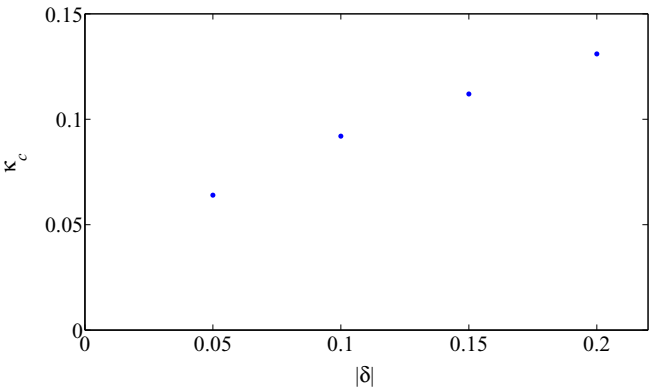

FIG. 4. (Color online) Numerically computed value of critical value κ_c (above which the sweet spot disappears) as a function of $|\delta|$, in the case $\delta < 0$.

where $\omega_L^0 = \mu_B B_m^0/(2\hbar)$. Physically, κ is linked to the degree of mixing in the dressed state picture [36]. The initial sign S of the detuning Δ_1, as described in Secs. III C and IV, is equal in this case to the sign of δ. The microwave field will be repulsive for $\delta > 0$, and attractive in the opposite case. Equations (15) and (16) can be used to plot the energy difference $V_b - V_a$ as a function of B, for different values of δ and κ, and find the minimum when applicable.

In Fig. 3 we show the case of an attractive microwave field by setting $\delta = -0.1$. In this case we observe that the sweet spot value increases with κ, up to a critical value on the order of $\kappa_c \simeq 0.092$, where the minimum disappears. The value of κ_c is observed to be a growing function of $|\delta|$, as illustrated in Fig. 4. This will result, in the attractive case, in a trade-off between the maximum Rabi frequency that can be used and the minimum detuning of the microwave frequency.

Let us now consider the opposite situation of a repulsive microwave field by setting $\delta = 0.1$. In this case, a minimum of $V_b - V_a$ is found even for values of κ much larger than unity, which is illustrated in Fig. 5 for $0 \leqslant \kappa \leqslant 1$. The situation remains the same for arbitrarily small values of $\delta > 0$, which shows that the repulsive case is much more favorable than the attractive case, because it allows the Rabi frequency and the detuning to be chosen independently without compromising the existence of a sweet spot.

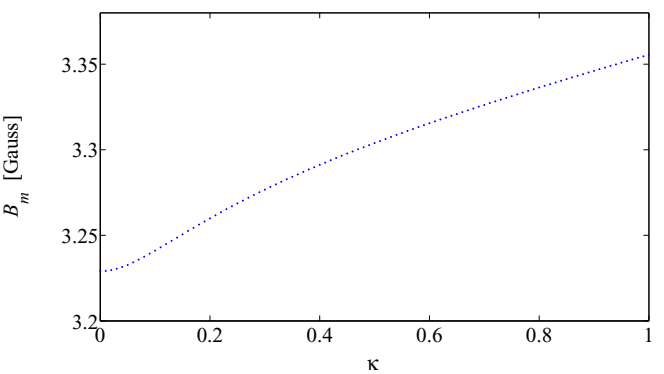

FIG. 5. (Color online) Numerically computed value of the sweet spot B_m as a function of κ, with $\delta = 0.1$.

VI. CONCLUSION

In conclusion, we have analyzed an experimental protocol for a symmetrical atom interferometer, based on the use of microwave dressing with two independent coplanar waveguide carrying different frequencies on an atom chip. We have pointed out the importance of symmetry for the contrast decay of a thermal atom interferometer in the framework of a simple model, and derived an analytical formula for the coherence time in the harmonic case. This study shows that it is preferable to use a repulsive (rather than attractive) microwave field (i.e., $\delta > 0$ with the notations used in this paper), because it avoids the problem of trap opening discussed in Sec. IV, reduces the degree of mixing κ by confining the atoms in a region of weaker microwave fields, and ensures the existence of a sweet spot to reduce the sensitivity to magnetic field fluctuations even for strong microwave dressing fields.

A significant asset of this two-frequency protocol is that it provides independent control over the potentials seen by the two states. This feature gives additional degrees of freedom to counteract the residual dissymmetry, due for example to the effect of far off-resonance transitions that we have neglected in this paper.

Interferometry between internal states of thermal atoms on a chip has been shown to hold great promise for realizing compact cold atom clocks [42]. If experimentally successful, an atom chip interferometer with trapped thermal atoms could be an important step towards the achievement of a new class of compact integrated inertial sensors.

ACKNOWLEDGMENTS

The authors would like to thank A. Sinatra and I. Carusotto for useful discussions at the beginning of the project. This work has been carried out within the CATS project ANR-09-NANO-039 funded by the French National Research Agency (ANR) in the frame of its 2009 program in Nano-science, Nanotechnologies, and Nanosystems (P3N2009) and within the OnACIS project ANR-13-ASTR-0031 funded by the French National Research Agency (ANR) in the frame of its 2013 Astrid program.

[1] A. D. Cronin, J. Schmiedmayer, and D. E. Pritchard, Optics and interferometry with atoms and molecules, Rev. Mod. Phys. **81**, 1051 (2009).

[2] A. Wicht, J. M. Hensley, E. Sarajlic, and S. Chu, A preliminary measurement of the fine structure constant based on atom interferometry, Phys. Scr. **2002**, 82 (2002).

[3] R. Bouchendira, P. Cladé, S. Guellati-Khélifa, F. Nez, and F. Biraben, New determination of the fine structure constant and test of the quantum electrodynamics, Phys. Rev. Lett. **106**, 080801 (2011).

[4] G. Lamporesi, A. Bertoldi, L. Cacciapuoti, M. Prevedelli, and G. M. Tino, Determination of the Newtonian gravitational constant using atom interferometry, Phys. Rev. Lett. **100**, 050801 (2008).

[5] A. Peters, K. Y. Chung, and S. Chu, High-precision gravity measurements using atom interferometry, Metrologia **38**, 25 (2001).

[6] J. M. McGuirk, G. T. Foster, J. B. Fixler, M. J. Snadden, and M. A. Kasevich, Sensitive absolute-gravity gradiometry using atom interferometry, Phys. Rev. A **65**, 033608 (2002).

[7] T. L. Gustavson, A. Landragin, and M. A. Kasevich, Rotation sensing with a dual atom-interferometer Sagnac gyroscope, Class. Quantum Gravity **17**, 2385 (2000).

[8] S. Dimopoulos, P. W. Graham, J. M. Hogan, and M. A. Kasevich, General relativistic effects in atom interferometry, Phys. Rev. D **78**, 042003 (2008).

[9] A. Bonnin, N. Zahzam, Y. Bidel, and A. Bresson, Simultaneous dual-species matter-wave accelerometer, Phys. Rev. A **88**, 043615 (2013).

[10] G. M. Tino, F. Sorrentino, D. Aguilera, B. Battelier, A. Bertoldi, Q. Bodart, K. Bongs, P. Bouyer, C. Braxmaier, L. Cacciapuoti, N. Gaaloul, N. Grlebeck, M. Hauth, S. Herrmann, M. Krutzik, A. Kubelka, A. Landragin, A. Milke, A. Peters, E. M. Rasel, E. Rocco, C. Schubert, T. Schuldt, K. Sengstock, and A. Wicht, Precision gravity tests with atom interferometry in space, Nucl. Phys. B **243-244**, 203 (2013).

[11] J. Reichel, W. Hänsel, and T. W. Hänsch, Atomic micromanipulation with magnetic surface traps, Phys. Rev. Lett. **83**, 3398 (1999).

[12] R. Folman, P. Krüger, D. Cassettari, B. Hessmo, T. Maier, and J. Schmiedmayer, Controlling cold atoms using nanofabricated surfaces: Atom chips, Phys. Rev. Lett. **84**, 4749 (2000).

[13] J. Fortágh and C. Zimmermann, Magnetic microtraps for ultracold atoms, Rev. Mod. Phys. **79**, 235 (2007).

[14] J. Reichel and V. Vuletić (eds.), *Atom Chips* (John Wiley and Sons, New York, 2010).

[15] T. van Zoest, N. Gaaloul, Y. Singh, H. Ahlers, W. Herr, S. T. Seidel, W. Ertmer, E. Rasel, M. Eckart, E. Kajari *et al.*, Bose-Einstein condensation in microgravity, Science **328**, 1540 (2010).

[16] W. Maineult, C. Deutsch, K. Gibble, J. Reichel, and P. Rosenbusch, Spin waves and collisional frequency shifts of a trapped-atom clock, Phys. Rev. Lett. **109**, 020407 (2012).

[17] A. Zatezalo, V. Vuletić, P. Baker, and T. C. Poling, Bose-Einstein Interferometry and Its Applications to Precision Undersea Navigation, in *Position, Location and Navigation Symposium, 2008 IEEE/ION* (IEEE, New York, 2008), pp. 940–950.

[18] Y. Shin, C. Sanner, G.-B. Jo, T. A. Pasquini, M. Saba, W. Ketterle, D. E. Pritchard, M. Vengalattore, and M. Prentiss, Interference of Bose-Einstein condensates split with an atom chip, Phys. Rev. A **72**, 021604 (2005).

[19] T. Schumm, S. Hofferberth, L. Mauritz Andersson, S. Wildermuth, S. Groth, I. Bar-Joseph, J. Schmiedmayer, and P. Krüger, Matter-wave interferometry in a double well on an atom chip, Nat. Phys. **1**, 57 (2005).

[20] P. Treutlein, T. W. Hänsch, J. Reichel, A. Negretti, M. A. Cirone, and T. Calarco, Microwave potentials and optimal control for robust quantum gates on an atom chip, Phys. Rev. A **74**, 022312 (2006).

[21] G.-B. Jo, Y. Shin, S. Will, T. A. Pasquini, M. Saba, W. Ketterle, D. E. Pritchard, M. Vengalattore, and M. Prentiss, Long phase

coherence time and number squeezing of two Bose-Einstein condensates on an atom chip, Phys. Rev. Lett. **98**, 030407 (2007).

[22] P. Böhi, M. F. Riedel, J. Hoffrogge, J. Reichel, T. W. Hänsch, and P. Treutlein, Coherent manipulation of Bose-Einstein condensates with state-dependent microwave potentials on an atom chip, Nat. Phys. **5**, 592 (2009).

[23] K. Maussang, G. E. Marti, T. Schneider, P. Treutlein, Y. Li, A. Sinatra, R. Long, J. Estève, and J. Reichel, Enhanced and reduced atom number fluctuations in a BEC splitter, Phys. Rev. Lett. **105**, 080403 (2010).

[24] F. Baumgärtner, R. J. Sewell, S. Eriksson, I. Llorente-Garcia, J. Dingjan, J. P. Cotter, and E. A. Hinds, Measuring energy differences by BEC interferometry on a chip, Phys. Rev. Lett. **105**, 243003 (2010).

[25] T. Berrada, S. van Frank, R. Bücker, T. Schumm, J.-F. Schaff, and J. Schmiedmayer, Integrated Mach-Zehnder interferometer for Bose-Einstein condensates, Nat. Commun. **4**, 2077 (2013).

[26] T. J. Davis, 2d magnetic traps for ultra-cold atoms: A simple theory using complex numbers, Eur. Phys. J. D. **18**, 27 (2002).

[27] O. Zobay and B. M. Garraway, Two-dimensional atom trapping in field-induced adiabatic potentials, Phys. Rev. Lett. **86**, 1195 (2001).

[28] M. Lewenstein and L. You, Quantum phase diffusion of a Bose-Einstein condensate, Phys. Rev. Lett. **77**, 3489 (1996).

[29] J. Javanainen and M. Wilkens, Phase and phase diffusion of a split Bose-Einstein condensate, Phys. Rev. Lett. **78**, 4675 (1997).

[30] J. Grond, U. Hohenester, I. Mazets, and J. Schmiedmayer, Atom interferometry with trapped Bose–Einstein condensates: Impact of atom–atom interactions, New J. Phys. **12**, 065036 (2010).

[31] E. Andersson, T. Calarco, R. Folman, M. Andersson, B. Hessmo, and J. Schmiedmayer, Multimode interferometer for guided matter waves, Phys. Rev. Lett. **88**, 100401 (2002).

[32] C. Cohen-Tannoudji and D. Guéry-Odelin, *Advances in Atomic Physics* (World Scientific, Singapore, 2011).

[33] C. Pethick and H. Smith, *Bose-Einstein Condensation in Dilute Gases* (Cambridge University Press, Cambridge, 2002).

[34] M. V. Berry, Quantal phase factors accompanying adiabatic changes, Proc. R. Soc. London Ser. A **392**, 45 (1984).

[35] D. M. Harber, H. J. Lewandowski, J. M. McGuirk, and E. A. Cornell, Effect of cold collisions on spin coherence and resonance shifts in a magnetically trapped ultracold gas, Phys. Rev. A **66**, 053616 (2002).

[36] J. Dalibard and C. Cohen-Tannoudji, Dressed-atom approach to atomic motion in laser light: The dipole force revisited, J. Opt. Soc. Am. B **2**, 1707 (1985).

[37] C. Cohen-Tannoudji, J. Dupont-Roc, and G. Grynberg, *Processus Dinteraction Entre Photons et Atomes* (InterEditions/Editions du CNRS, Paris, 1992).

[38] P. Treutlein, Coherent manipulation of ultracold atoms on atom chips, Ph.D. thesis, Ludwig Maximilians Universität München, 2008.

[39] T. Schumm, Bose-Einstein condensates in magnetic double well potentials, Ph.D. thesis, Université Paris 11, 2005.

[40] D. A Steck, Rubidium 87 *d* line data, 2003, http://steck.us/alkalidata.

[41] P. Treutlein, P. Hommelhoff, T. Steinmetz, T. W. Hänsch, and J. Reichel, Coherence in microchip traps, Phys. Rev. Lett. **92**, 203005 (2004).

[42] C. Deutsch, F. Ramirez-Martinez, C. Lacroûte, F. Reinhard, T. Schneider, J.-N. Fuchs, F. Piéchon, F. Laloë, J. Reichel, and P. Rosenbusch, Spin self-rephasing and very long coherence times in a trapped atomic ensemble, Phys. Rev. Lett. **105**, 020401 (2010).